

PNAS

www.pnas.org

1

2 Main Manuscript for

3 Rate of atmospheric brown carbon whitening governed by
4 environmental conditions

5

6 Elijah G. Schnitzler^{a,1,2}, Nealan G. A. Gerrebos^{b,1}, Therese S. Carter^c, Yuanzhou Huang^b, Colette
7 L. Heald^{c,d,3}, Allan K. Bertram^{b,3}, and Jonathan P. D. Abbatt^{a,3}

8 ^aDepartment of Chemistry, University of Toronto, Toronto, M5S 3H6, Canada; ^bDepartment of
9 Chemistry, University of British Columbia, Vancouver, V6T 1Z1, Canada; ^cCivil and
10 Environmental Engineering Department, Massachusetts Institute of Technology, Cambridge,
11 02139, USA; ^dEarth, Atmospheric and Planetary Sciences, Massachusetts Institute of
12 Technology, Cambridge, 02139, USA

13 ¹E.G.S. and N.G.A.G. contributed equally to this work.

14 ²Present address: Department of Chemistry, Oklahoma State University, Stillwater, 74078, USA

15 ³To whom correspondence may be addressed. Email: jonathan.abbatt@utoronto.ca,
16 bertram@chem.ubc.ca, or heald@mit.edu.

17 **Author Contributions:** E.G.S., C.L.H., A.K.B., and J.P.D.A. designed research; E.G.S.,
18 N.G.A.G., T.S.C., Y.H. performed research; E.G.S., N.G.A.G., T.S.C., Y.H. analyzed data;
19 E.G.S., N.G.A.G., T.S.C., Y.H., C.L.H., A.K.B., and J.P.D.A. wrote the paper.

20 **Competing Interest Statement:** The authors disclose no competing interest.

21 **Classification:** Earth, Atmospheric, and Planetary Sciences.

22 **Keywords:** biomass burning, organic aerosol, brown carbon, multiphase chemistry, aerosol
23 kinetics.

24

25 **This PDF file includes:**

26 Main Text
27 Figures 1 to 3

28 **Abstract**

29 Biomass burning organic aerosol (BBOA) in the atmosphere contains many compounds that absorb
30 solar radiation, called brown carbon (BrC). While BBOA is in the atmosphere, BrC can undergo
31 reactions with oxidants such as ozone which decrease absorbance, or whiten. The effect of
32 temperature and relative humidity (RH) on whitening has not been well constrained, leading to
33 uncertainties when predicting the direct radiative effect of BrC on climate. Using an aerosol flow-
34 tube reactor, we show that the whitening of BBOA by oxidation with ozone is strongly dependent
35 on RH and temperature. Using a poke-flow technique, we show that the viscosity of BBOA also
36 depends strongly on these conditions. The measured whitening rate of BrC is described well with
37 the viscosity data, assuming that the whitening is due to oxidation occurring in the bulk of the BBOA,
38 within a thin shell beneath the surface. Using our combined datasets, we developed a kinetic model
39 of this whitening process, and we show that the lifetime of BrC is 1 day or less below approximately
40 1 km in altitude in the atmosphere but is often much longer than 1 day above this altitude. Including
41 this altitude dependence of the whitening rate in a chemical transport model causes a large change
42 in the predicted warming effect of BBOA on climate. Overall, the results illustrate that RH and
43 temperature need to be considered to understand the role of BBOA in the atmosphere.

44 **Significance Statement**

45 Biomass burning organic aerosol (BBOA) has a significant direct effect on climate by absorbing
46 solar radiation. Understanding this effect is increasingly important as wildfires become more
47 prevalent in several regions across the globe. While transported in the atmosphere, BBOA can
48 react with atmospheric oxidants, leading to less-absorbing products, or whitening. We show that
49 this whitening is strongly influenced by relative humidity and temperature and, consequently,
50 vertical transport in the atmosphere. Implementing altitude-dependent whitening of BBOA in a
51 global atmospheric model indicates that the effects of changing environmental conditions need to
52 be included when simulating the direct climate effects of BBOA.

53
54 **Main Text**

55 **Introduction**

56 Biomass burning is a significant source of organic aerosol to the atmosphere, and the mass of this
57 aerosol is expected to increase in the future as forest fires increase in occurrence across diverse
58 regions due to climate change (1, 2). Biomass burning organic aerosol (BBOA) contains a
59 significant amount of light-absorbing material, referred to as brown carbon (BrC). This light-
60 absorbing material exerts a positive radiative effect on Earth's climate, leading to a strong warming
61 effect, dictated in part by its lifetime in the atmosphere (3–5).

62 In the atmosphere, BrC is susceptible to a wide range of chemical aging processes, in
63 addition to dilution (6, 7), such as photolysis and heterogeneous oxidation with OH, O₃, and NO₃,
64 which alter its light-absorption properties (8–13). After an initial period when darkening may occur
65 (13, 14), steady whitening (i.e., decreasing absorbance) of BrC occurs for some conditions found
66 in the troposphere (15–18). For example, in two studies, the light absorption of BrC was observed
67 to decrease exponentially with transport time with a timescale of about 1 day (15, 19), and this
68 evolution is associated with changes in composition, including an increase in the oxidation level of
69 BBOA (15, 20) and the degradation of small chromophores (21, 22), like nitrophenols (23, 24). On
70 the other hand, for BrC in a convection outflow at high altitude, no whitening was observed after
71 one day of subsequent aging (25).

72 Heat from biomass burning sources can enhance vertical transport by convection and
73 result in the formation of pyrocumulus and pyrocumulonimbus clouds (26, 27), such that BrC from
74 wildfires can be transported to the middle and upper troposphere and even the lower stratosphere
75 (25, 28–30). As BBOA is transported vertically, it is exposed to rapidly changing environmental

79 conditions, signified by the lapse rate of -6.5 K km^{-1} . Relative humidity (RH) also fluctuates with
80 altitude, although not uniformly. Overall, the effect of RH and temperature on the lifetime of BrC is
81 poorly constrained, leading to uncertainty when predicting the radiative effect of BrC on climate.
82 The phase state of organic aerosol is strongly dependent on temperature and RH (31–34).
83 Secondary organic aerosol (SOA) in particular is modelled to be in a glassy state across the globe
84 at altitudes greater than 5 km (35, 36), and primary BBOA will likely respond similarly to the rapidly
85 changing environmental conditions upon vertical transport. If BBOA is solid or highly viscous, slow
86 diffusion of organic species and oxidants within the particles will limit reactivity (37, 38). If BrC is
87 long-lived in the middle and upper troposphere, then its overall radiative effect may be larger than
88 previously expected (39, 40).

89 Here, we report complementary laboratory experiments, kinetic simulations, and global
90 model simulations to determine the effect of RH and temperature on the time scales for whitening
91 of BrC by heterogeneous reaction with ozone throughout the troposphere and to assess the impact
92 of BrC on Earth's radiative balance. Water-soluble BBOA samples were generated by controlled
93 smoldering of wood. The whitening of the BrC component was investigated across a range of RH
94 and temperature conditions relevant to the free troposphere, from the planetary boundary layer
95 (PBL) at about 1 km to the tropopause, using a cooled flow tube, in which RH was precisely
96 controlled down to 253 K. The viscosity of the BBOA was investigated across a range of RH
97 conditions using the poke-flow technique (41), and the viscosity measurements were used to
98 develop a parameterization of viscosity as a function of RH and temperature. Based on this
99 parameterization, kinetic simulations of the experimental data provide insights into the mechanism
100 of the reaction, and they inform global chemical transport model simulations that were performed
101 to assess the direct radiative effect (DRE) of BrC on climate.

104 Results and Discussion

105 **Whitening of BrC as a Function of RH and Temperature.** BBOA contains a wide range of
106 phenolic molecules, originating from the thermal degradation of lignin, including species such as
107 sinapaldehyde and coniferaldehyde (42, 43). These representative species with exocyclic carbon-
108 carbon double bonds are reactive with ozone (44, 45) and exhibit marked visible-light absorption
109 (43). To determine the reactivity of BrC with ozone, laboratory-generated pine BBOA was extracted
110 into water and aerosolized, and the resulting submicron particles, with a geometric mean diameter
111 of about 100 nm, were exposed to ozone in a reaction flow tube, equipped with precise RH and
112 temperature control, as shown in Fig. S1 (see Materials and Methods).

113 The metric used for reactivity was relative absorption at 405 nm, measured for suspended
114 particles downstream of the flow tube using a photoacoustic spectrometer. Relative absorption was
115 quantified by comparing measurements of the absorption coefficient at 405 nm when ozone was
116 present to those when ozone was absent. A representative time series of the absorption coefficient
117 at 405 nm, shown in Fig. S2, at 273 K and 20, 40, and 60% RH depicts the appreciable and variable
118 extent of whitening that occurred due to exposure to ozone. In contrast to the absorption coefficient,
119 the size distribution did not change upon ozone exposure (e.g., Fig. S3). Throughout the flow-tube
120 experiments, there was no evidence of particle growth or volatilization. Consequently, the observed
121 decay in relative absorption was due to changes in the composition and absorptivity of the water-
122 soluble BBOA, rather than changes in the particle size.

123 To compare whitening across a broad range of temperature and RH conditions, the relative
124 absorption remaining after exposure to a high mixing ratio of ozone, 45 ppm, was measured at 253-
125 293 K and 5-80% RH, with a fixed aerosol residence time of 130 s. The results of these experiments
126 are summarized in Fig. 1A. For all temperatures, a strong dependence on RH was observed, with
127 the amount of whitening decreasing with RH. For example, at 293 K, the absorption decreases by
128 more than 40% at 60% RH but less than 5% at 5% RH. The amount of whitening was also strongly
129 dependent on temperature. For example, at 60% RH, the extent of whitening went from more than
130 40% at 293 K to about 30% at 273 K and less than 10% at 253 K. Furthermore, at the lowest
131 temperature, 253 K, and RH values less than or equal to 40%, the extent of whitening was too

133 small to detect in our experiment, illustrating that whitening time scales can be long at low
134 temperature and low RH.

135 Relative absorption as a function of ozone mixing ratio was also measured for two
136 temperatures and two relative humidities, yielding the results shown in Fig. 1B. At the given
137 temperature and RH values, the relative absorption decreased as the ozone mixing ratio increased
138 from roughly 5 to 45 ppm. At low ozone mixing ratios, there is no indication of absorption
139 enhancement due to oxidation, associated with a relative absorption greater than one, so
140 heterogeneous ozone oxidation led only to the whitening of the water-soluble BBOA considered
141 here. Previously, exposure of BBOA extracts from the same source to aqueous OH radicals in bulk
142 solutions led to an initial absorption enhancement at 400 nm, followed by slower, steady whitening
143 (46). Similarly, exposure of whole suspended BBOA from the same source to gas-phase OH
144 radicals led to absorption enhancement followed by whitening (8). On the other hand, exposure of
145 whole suspended and filter-deposited BBOA from other sources to gas-phase ozone led only to
146 whitening (9, 47), as observed here. Together, these observations suggest that the distinct optical
147 evolution due to ozone relates to the identity of the oxidant rather than the composition of the BBOA
148 in which the reaction occurs. The light-absorbing molecules that react with ozone may include
149 sinapaldehyde, coniferaldehyde, and larger species with exocyclic carbon-carbon double bonds,
150 which will be fragmented by the addition of ozone across the double bond. Electron-rich aromatic
151 rings may also be reactive to ozone. Since whitening is observed without an accompanying change
152 in particle size, the mass fraction of these species may be small, although they contribute a
153 significant fraction of the total absorption.

154 The effects of RH and temperature, in addition to ozone mixing ratio, are also evident in
155 Fig. 1B. Most apparent, the decay in the relative absorption was much faster at 293 K than at 273
156 K. At 293 K, the relative absorption reached an asymptote of 50% of the initial absorption at an
157 ozone mixing ratio of 45 ppm, above which no additional whitening is expected. At 273 K, the
158 relative absorption was still decreasing at 45 ppm, approaching the same asymptote. Previously,
159 studies have suggested that a significant fraction of the light-absorbing species in whole BBOA
160 from pine needle litter was either unreactive with ozone or physically protected from ozone at room
161 temperature and 30% RH (9). The asymptote here similarly reflects the water-soluble BBOA
162 constituents that are recalcitrant with respect to ozone, which account for 50% of the initial
163 absorption.

164 **Viscosity of BBOA as a Function of RH and Temperature.** Reaction rates between organic
165 aerosol constituents and gas-phase oxidants, including ozone, are governed in part by the viscosity
166 of the particles (48). Viscosities of the water-soluble BBOA considered here were measured using
167 the poke-flow technique (see Materials and Methods), allowing estimates of diffusion coefficients
168 within the water-soluble BBOA and, in turn, insights into the reaction rates between BrC and ozone
169 in the atmosphere and in the laboratory (i.e., flow-tube) experiments. Micrographs from poke-flow
170 measurements for filter-collected BBOA extracted into water are shown in Fig. S4. Experiments
171 were performed at 294 K and 0–25% RH, and images from representative experiments at 0 and
172 25% RH are presented. Before being poked with a needle, the droplets were spherical in shape.
173 Upon being poked, they adopted a half-torus geometry. With the needle removed, the droplets
174 began to flow in order to decrease their surface energy, with a characteristic experimental recovery
175 time, $\tau_{\text{exp, flow}}$. The experimental recovery time decreased significantly as RH increased, such that
176 it was on the order of 1000 s at 0% RH and 10 s at 25% RH, as shown in Fig. S5.

177 The viscosities determined from these experimental flow times using fluid dynamic
178 simulations are shown in Fig. 2A. The viscosity of the samples at 0% RH was approximately $1–2 \times$
179 10^5 Pa s. For reference, the viscosity of peanut butter is approximately 1×10^3 Pa s, and the
180 viscosity of tar pitch is approximately 1×10^8 Pa s (34). As the RH increased from 0% to 25%, the
181 viscosity decreased by approximately a factor of 100. A decrease in viscosity with an increase in
182 RH is expected since the water content of the BBOA is expected to increase, and water is known

184 to be a plasticizer (i.e., the presence of water leads to a decrease in viscosity in highly viscous
185 material (34)).

186 The viscosity data above were used to develop a parameterization of viscosity as a function
187 of temperature and RH for BBOA (SI Appendix, section S1). The parameterization applies a mole-
188 fraction-based Arrhenius mixing rule to describe viscosity as a function of RH and the Vogel-
189 Folcher-Tamman equation to describe viscosity as a function of temperature, as has been done
190 previously (35, 36, 49). The viscosity as a function of RH and temperature determined with this
191 procedure is shown in Fig. 2B. Similar to the whitening experiments, a strong dependence on both
192 RH and temperature is observed.

193
194 **Analysis of BrC Whitening Kinetics Using the Viscosity Parameterization.** The rate of
195 whitening of BrC within the BBOA particles by ozone can be limited by several processes, including
196 surface and bulk reaction rates between reactive BrC and ozone, solubility of ozone within the
197 particles, and diffusion of ozone and BrC within the particles. The resistor model is a simple way to
198 understand and account for these processes. If the reaction between ozone and BrC is fast and
199 occurs in a thin layer near the surface, the reactivity of BrC within the particle can be described by
200 the following equation based on the resistor model (50):

$$202 \sqrt{\frac{[BrC](t)}{[BrC]_0}} = 1 - \frac{3RTn_{O_3}(g)H\sqrt{D_{O_3}k_2}}{2a\sqrt{[BrC]_0}} t \quad [1]$$

203 where $[BrC]_0$ is the initial concentration of BrC, R is the gas constant, T is the temperature, n_{O_3} is
204 the concentration of ozone in the gas phase, H is Henry's law constant, D_{O_3} is the diffusion
205 coefficient of ozone within the particles, k_2 is the second order rate coefficient for the ozonolysis of
206 BrC within the particles, a is the radius of the aerosol particles, and t is the time. Eq. 1 assumes
207 that BrC is uniform throughout the particles during ozonolysis. A time scale analysis using
208 estimated diffusion coefficients of BrC within the particles is consistent with this assumption (SI
209 Appendix, Section S2).

210 Eq. 1 can be rewritten in terms of ozone partial pressure, P_{O_3} (51), as shown in the SI
211 Appendix (section S3). The fraction of BrC that remains unreacted was assumed to be equivalent
212 to the absorption relative to the initial absorption, Abs_t/Abs_0 . Furthermore, Abs_t/Abs_0 was forced to
213 be $\geq 50\%$ since the absorption of BrC never falls below approximately 50% of the initial value,
214 regardless of RH or temperature (Fig. 1). Rearrangement of Eq. 1 and these constraints lead to the
215 following equation:

$$217 \frac{Abs_t}{Abs_0} = 0.5 \left(1 - \frac{3H\sqrt{D_{O_3}k_2}}{2a\sqrt{[BrC]_0}} P_{O_3} t \right)^2 + 0.5 \quad [2]$$

218 Eq. 2 was fit to the experimental measurements of relative absorption of BrC as a function of RH
219 (Fig. 1A) and O₃ mixing ratio (Fig. 1B) to obtain $H(k_2/[BrC]_0)^{1/2}$ at temperatures of 253, 273, and
220 293 K (Fig. S7). For t and a , values of 130 s and 143 nm were used, based on the residence time
221 and median volume radius of the particles used in the flow tube experiments. D_{O_3} was calculated
222 using the parameterization for viscosity as a function of RH and temperature and the fractional
223 Stokes-Einstein equation (52), as discussed in the SI Appendix (section S3). Shown in Fig. 1A are
224 the fits of Eq. 2 to the experimental data for the unreacted BrC fraction as a function of RH at 293,
225 273, and 253 K. For these experiments, $P_{O_3} = 4.5 \times 10^{-5}$ atm (45 ppm). Shown in Fig. 1B are the fits
226 of Eq. 2 to the experimental data of Abs_t/Abs_0 as a function of O₃ mixing ratio at 293 and 273 K
227 and 60 and 80% RH.

228 The good agreement between the experimental data and the fits to Eq. 2 in Fig. 1 is
229 consistent with the reaction between O₃ and BrC occurring in the bulk of the BBOA, within a thin
230 shell below the surface (50). Shown in Fig. S7 are the $H(k_2/[BrC]_0)^{1/2}$ values determined from the
231 fits of Eq. 2 to the experimental data. There is not a strong dependence on temperature. A change
232 in the reaction rate constant k_2 is expected, but it could be compensated for by a change in H .
233 Furthermore, the $H(k_2/[BrC]_0)^{1/2}$ values determined from the fits are consistent with values

234 estimated based on literature data (SI Appendix, Section S4). The line in Fig. S7 represents a linear
235 fit of the $H(k_2/[BrC]_0)^{1/2}$ values as a function of temperature, and it was used when predicting the
236 lifetime of BrC in the atmosphere, together with Eq. 1 (see below).

237 In addition to the analysis above, we also investigated if other model representations
238 previously used to describe reactivity of particles were able to describe our experimental data well.
239 For example, we compared the experimental data in Fig. 1a to predictions using the resistor model
240 and assuming the reaction between O_3 and BrC was limited by only diffusion of BrC within the
241 particles (SI Appendix, Section S5). In this case, the agreement between the experimental data
242 and the predictions was poor (SI Appendix, Section S5). In addition, we considered the resistor
243 model and assuming O_3 and BrC were well-mixed throughout the particles (SI Appendix, Section
244 S6). In this case, good agreement between the experimental data and model representation was
245 only obtained if unrealistic values of H and k_2 are used (SI Appendix, Section S6). We conclude
246 that the model representation we used to describe our data (i.e., Eq. 1) is a reasonable
247 representation of our data since the data is described well by Eq. 1, the $H(k_2/[BrC]_0)^{1/2}$ values
248 extracted from our fits are consistent with expectations, and two other model representations
249 previously used to describe reactive uptake do not describe our data well.

250
251 **Predictions of Lifetime and Direct Radiative Impacts of BrC in the Atmosphere.** The lifetime
252 of reactive BrC in the atmosphere due to this aging process influences its radiative effect and
253 environmental impact. From Eq. 1, the lifetime, τ_{BrC} , can be expressed as the following:
254

$$255 \quad \tau_{BrC} = \frac{\left(1 - \frac{1}{\sqrt{e}}\right) 2a \sqrt{[BrC]_0}}{3HP_{O_3} \sqrt{D_{O_3}} k_2} \quad [3]$$

256 To calculate τ_{BrC} as a function of altitude and latitude in the atmosphere, first, annual
257 average temperature and RH values as a function of altitude and latitude in the atmosphere were
258 determined from MERRA2 data (40). Next, D_{O_3} as a function of altitude and latitude in the
259 atmosphere was calculated using these temperature and RH fields, the fractional Stokes-Einstein
260 equation, and our parameterization of viscosity as a function of temperature and RH (Fig. 2B).
261 Finally, τ_{BrC} was calculated as a function of altitude and latitude using the D_{O_3} values as a function
262 of altitude and latitude, the derived values for $H(k_2/[BrC]_0)^{1/2}$ (line in Fig. S7) and Eq. 3. For the latter
263 calculation, the following variables were used: $a = 150$ nm and $P_{O_3} = 3.5 \times 10^{-8}$ atm, i.e., 35 ppb of
264 ozone. The partial pressure of ozone was based on an average of measurements of tropospheric
265 ozone at surface level and at 10 km, multiplied by the atmospheric pressures at the same altitudes
266 (53–57). The radius was chosen based on volume size distributions of atmospheric BBOA (58–60).
267 $H(k_2/[BrC]_0)^{1/2}$ was calculated at each temperature using the fit in Fig. S7, giving a value of
268 approximately $9 \text{ atm}^{-1} \text{ s}^{-1/2}$ at all temperatures in the range evaluated.

269 Shown in Fig. 3A are the τ_{BrC} values as a function of altitude and latitude calculated with
270 this approach, including the altitude corresponding to a τ_{BrC} of 1 day. The zonally averaged altitude
271 for this lifetime is similar to the height of the PBL, i.e., very roughly 1 km. Throughout much of the
272 mid- and upper troposphere, the whitening lifetime via this process is considerably longer than a
273 typical particle residence time, which is often taken as roughly a week (61, 62). Indeed, for ozone,
274 a fraction of the BBOA BrC was recalcitrant to whitening.

275 What is the impact of this altitude-dependent whitening process of BBOA BrC on its global
276 concentration and DRE? To answer this question, a global three-dimensional chemical transport
277 model, GEOS-Chem, was coupled to the RRTMG radiative transfer model (63) in a configuration
278 known as GC-RT (64). The zonal concentration of BrC in the northern hemisphere (NH) and tropics
279 is highest below 2.5 km, while in the southern hemisphere (SH), it is highest in the upper
280 troposphere, as shown in Fig. 3C. As illustrated in Carter et al. (40), with no whitening included in
281 the model, the global annual mean top-of-the-atmosphere DRE of BrC is 0.29 W m^{-2} and drops to

282 0.08 W m⁻² when including whitening with a lifetime of 1 day at all altitudes (Fig. 3B; also see Fig. 283 S8).

284 When a whitening lifetime (of 1 day) is included only at altitudes below 1 km, in agreement 285 with the current experimental results, the decrease in BrC concentration depends more strongly on 286 region, with a significant decrease only in the NH (Fig. 3C; also see Fig. S8). At high latitudes, 287 where the PBL in fire regions is nearly always below 1 km, emitted BrC is efficiently whitened within 288 the PBL, substantially decreasing BrC concentrations exported to the free troposphere. In the 289 tropics, a deeper PBL allows BrC to be lofted above the whitening zone, leading to overall less 290 efficient whitening. When limiting the whitening process to below 1 km, the decrease in the global 291 DRE is less pronounced, reaching about 0.17 W m⁻², indicating that increased aerosol viscosity at 292 high altitudes enhances the warming effect of BrC.

293 **Atmospheric Implications.** This work uniquely combines measurements of aerosol reactivity and 294 viscosity with simulations of aerosol radiative effects to explore the critical impact of environmental 295 conditions on the whitening of BrC BBOA and its DRE. Together, the results demonstrate that the 296 timescale for whitening by ozone oxidation becomes longer than 1 day for altitudes greater than 297 roughly 1 km. We stress that the specific timescale and altitude threshold for whitening will depend 298 on a number of factors, including the size of the particles, environmental conditions, absorption 299 wavelengths, and the concentrations and identity of the oxidants. In this work, heterogeneous 300 oxidation by ozone of wood smoke was considered. Previous studies have shown that low 301 temperatures can also reduce the rate of BBOA chemical aging by hydroxyl radicals (33, 65); 302 although, the direct connection to the optical properties of the particles was not made in those 303 works. Low temperature NO₃ aging experiments have not yet been reported, nor have low 304 temperature photoreaction studies of BBOA; although, work using individual molecules (e.g., 305 nitrophenols) has shown slower photodegradation rates in organic matrices (66). In addition, the 306 nature of the BBOA BrC material should be varied in subsequent studies, to explore how this 307 whitening phenomenon depends on composition, combustion conditions, and BrC water solubility.

308 Although the derived aging timescale of 24 hours at about 1 km altitude in the atmosphere 309 may vary somewhat as a function of environmental conditions, BBOA composition, and aging 310 mechanism, the overall behavior demonstrated in this study is expected to be universal. In 311 particular, it is expected that BrC aging processes will be slowest in regions of the atmosphere 312 where the environmental conditions lead to high BBOA viscosity, such as the mid- and upper 313 troposphere. As shown in this work, this will have significant effects on the DRE of BrC. Past models 314 that have assumed a uniform BrC aging timescale of 1 day throughout the troposphere are likely 315 underestimating the BrC DRE (39, 40). Indeed, we note that the environmental conditions in much 316 of the mid- and upper troposphere lead to aging timescales of a week or more (Fig. 3A).

317 We finish by noting that the viscosity of BBOA may reach very high values, perhaps even 318 those of a glass, under some environmental conditions such as those in the upper troposphere 319 (Fig. 2B; see also Fig. S9 for a global distribution of viscosity and glass state of BBOA). The rates 320 of heterogeneous oxidation will be slower in more viscous particles, resulting in slower removal of 321 the BBOA particles via wet deposition. As well, previous results have shown that certain types of 322 glassy aerosol can act as ice nucleating particles and, hence, influence properties of clouds and 323 climate (67, 68). Since BBOA may be in a glassy state in the upper troposphere, studies are needed 324 to quantify the ice nucleation ability of glassy BBOA. Beyond effects on the DRE of BrC, which was 325 the main focus of this paper, this may be another mechanism by which environmental conditions 326 affect BBOA and its influence on climate.

328 329 **Materials and Methods** 330

331 **BBOA Generation and Collection.** Samples of BBOA were generated by controlled, low 332 temperature smoldering of untreated, commercial pine wood in a heated flow tube (46, 69, 70). 333 Clean air (Linde, Grade Zero 0.1) flowed through a quartz tube with an inner diameter of 2.2 cm at 334 a rate of 2.0 L min⁻¹. A 30.5-cm length of the tube rested in a tube furnace (Thermo, Lindberg Blue

335 M), and a 27.0-cm length extended downstream. Particles were collected on filters of borosilicate
336 glass bonded to PTFE (Pall, Emfab).

337 For a typical sample of BBOA, three rectangular chips of pine, with a total mass of about 6
338 g, were placed in the quartz tube, and the furnace temperature was ramped to 673 K. Filter
339 sampling began only after the wood had dried and once strong smoldering, with a distinct front,
340 was observed; care was taken to avoid flaming conditions. For filter sampling, typically about 100
341 mg of whole BBOA was collected.

342 **Heterogeneous Ozone Oxidation.** It was important to prepare the sample flow with the correct
343 RH at a specific temperature. To do this, the conditioned sample (SI Appendix, section S7) was
344 directed into a double-jacketed glass flow tube, called the RH-conditioner, as in Fig. S1. A
345 recirculating chiller filled with a mixture of ethylene glycol and water was connected to flow through
346 the inner jacket of this flow tube. RH was monitored at room temperature with a commercial probe
347 (VWR). For experiments conducted at 253 and 273 K, ultrapure water was added to the
348 conditioning flow tube, and its temperature was monitored continuously with a thermocouple. The
349 sample in the RH-conditioner is assumed to be at ice saturation (71), and the temperature was
350 adjusted such that the saturation vapor pressure of ice gave the desired RH once the sample was
351 directed into the adjacent reaction flow tube, also double-jacketed.

352 Near the inlet of the reaction flow tube, ozone was added to the sample, in a carrier gas
353 with a flow rate of 0.2 L min⁻¹, to give a total flow rate of 1.0 L min⁻¹ through the flow tube. With the
354 reaction volume, the residence time in the flow tube was 130 ± 10 s. The total aerosol mass loading
355 in the flow tube was about 1000 µg m⁻³. Ozone was generated by passing clean, dry air (Linde,
356 Grade Zero 0.1) through a small glass tube housing a Hg lamp at its center. The ozone mixing ratio
357 was varied by adjusting the shielding around the Hg lamp and was measured for the same total
358 flow rate using an ozone monitor (2B Technologies, 202). To allow as long a residence time as
359 possible in the flow tube and still provide sufficient aerosol absorption, ozone was not monitored
360 continuously. A second recirculating chiller filled with the same ethylene-water mixture was
361 connected to flow through the inner jacket of the reaction flow tube. The temperature was adjusted
362 and monitored with a second thermocouple, which was retracted from the flow tube once the Hg
363 lamp was turned on to introduce ozone. The RH in the reaction flow tube was calculated from its
364 temperature and the water content of the sample leaving the RH-conditioner.

365 **Particle Viscosity Measurement.** The viscosity of the aerosol particles nebulized and deposited
366 on a hydrophobic glass slide was determined using the poke-flow technique (32, 41, 72). During
367 the experiment, the slide and sample were placed inside a flow cell with both RH and temperature
368 control. The sample was conditioned overnight (>12 hr) at 294 ± 1 K, and the poke-flow
369 measurement was performed at 2, 4, and 6 hr after conditioning (within the uncertainties of the
370 measurements, the viscosities did not depend on the conditioning time used, as shown in Fig. S10).
371 The glass slide was mounted in the flow cell with a hole at the top through which a needle could be
372 inserted. The droplet was poked using a sharp needle (Ted Pella Company, 13561-20) coated with
373 hydrophobic oil slip coating (Cytonix, OilSlip 110). The needle was attached to a micromanipulator
374 stage, which allowed it to move in the x, y, and z directions.

375 In a typical experiment, the needle tip was aligned above the center of the droplet, and it
376 was slowly lowered until it touched the particle and was then quickly raised, leaving a depression
377 in the droplet and a shape similar to a half-torus geometry. The droplet began to flow to reduce its
378 surface energy and eventually returned to the original spherical geometry. The change in
379 morphology as a function of time was recorded with a CCD camera connected to a microscope
380 (AmScope). The experimental flow (or recovery) time, $\tau_{\text{exp, flow}}$, was defined as the time taken for
381 the equivalent area diameter of the hole to decrease to 50% of its original value. Fluid dynamic
382 simulations were performed as discussed in the SI Appendix (section S8).

383 **Global Transport and Radiative Transfer Modelling.** The BrC simulation employed GEOS-
384 Chem coupled to RRTMG (63) in a configuration known as GC-RT, v.12.3.0 (64), and was
385 compared to previous results from Carter et al. (40). Simulations were performed at 2.0 x 2.5 degree

389 horizontal resolution with 47 vertical levels and were driven by MERRA-2 meteorology. GFED4s
390 was used to represent fire emissions. It was assumed that 100% of BBOA was brown or absorbing
391 and that this was the only source of BrC. Details on BrC emissions and non-absorbing organic
392 aerosol optical properties used in the model are provided elsewhere (39, 73). The BrC absorption
393 properties vary based on the BC-to-OA ratio (40), following Saleh, et al. (74). The lifetime for BrC
394 whitening was treated as constant, set to 1 day. The whitening parameterization does not allow
395 BrC absorptivity to drop below 25% of the starting value. The global whitening and non-whitening
396 simulations reported previously (40) are compared with the new simulation based on the laboratory
397 results, in which whitening occurs only below 1 km.
398
399

400 **Acknowledgments**

401 This research was funded by the Natural Sciences and Engineering Research Council of Canada
402 (NSERC). E.G.S. gratefully acknowledges a postdoctoral fellowship from NSERC. C.L.H. and
403 T.S.C. acknowledge support from the U.S. National Science Foundation (NSF AGS 1936642).
404
405

406 **References**

- 408 1. P. E. Dennison, S. C. Brewer, J. D. Arnold, M. A. Moritz, Large wildfire trends in the western
409 United States, 1984–2011. *Geophysical Research Letters* **41**, 2928–2933 (2014).
- 410 2. J. G. Canadell, *et al.*, Multi-decadal increase of forest burned area in Australia is linked to
411 climate change. *Nat Commun* **12**, 6921 (2021).
- 412 3. R. Saleh, From Measurements to Models: Toward Accurate Representation of Brown
413 Carbon in Climate Calculations. *Curr Pollution Rep* (2020) <https://doi.org/10.1007/s40726-020-00139-3> (April 22, 2020).
- 415 4. C. E. Chung, V. Ramanathan, D. Decremer, Observationally constrained estimates of
416 carbonaceous aerosol radiative forcing. *PNAS* **109**, 11624–11629 (2012).
- 417 5. H. Brown, *et al.*, Biomass burning aerosols in most climate models are too absorbing.
418 *Nature Communications* **12**, 277 (2021).
- 419 6. N. M. Donahue, A. L. Robinson, C. O. Stanier, S. N. Pandis, Coupled Partitioning, Dilution,
420 and Chemical Aging of Semivolatile Organics. *Environ. Sci. Technol.* **40**, 2635–2643 (2006).
- 421 7. A. L. Hodshire, *et al.*, Dilution impacts on smoke aging: evidence in Biomass Burning
422 Observation Project (BBOP) data. *Atmospheric Chemistry and Physics* **21**, 6839–6855
423 (2021).
- 424 8. E. G. Schnitzler, T. Liu, R. F. Hems, J. P. D. Abbatt, Heterogeneous OH oxidation of primary
425 brown carbon aerosol: effects of relative humidity and volatility. *Environ. Sci.: Processes
426 Impacts* **22**, 2162–2171 (2020).
- 427 9. E. C. Browne, *et al.*, Effect of heterogeneous oxidative aging on light absorption by biomass
428 burning organic aerosol. *Aerosol Science and Technology* **53**, 663–674 (2019).

429 10. C. Li, *et al.*, Formation of Secondary Brown Carbon in Biomass Burning Aerosol Proxies
430 through NO₃ Radical Reactions. *Environ. Sci. Technol.* **54**, 1395–1405 (2020).

431 11. B. J. Sumlin, *et al.*, Atmospheric Photooxidation Diminishes Light Absorption by Primary
432 Brown Carbon Aerosol from Biomass Burning. *Environ. Sci. Technol. Lett.* **4**, 540–545
433 (2017).

434 12. Z. Cheng, *et al.*, Evolution of the light-absorption properties of combustion brown carbon
435 aerosols following reaction with nitrate radicals. *Aerosol Science and Technology* **54**, 849–
436 863 (2020).

437 13. J. P. S. Wong, *et al.*, Atmospheric evolution of molecular-weight-separated brown carbon
438 from biomass burning. *Atmospheric Chemistry and Physics* **19**, 7319–7334 (2019).

439 14. R. F. Hems, E. G. Schnitzler, C. Liu-Kang, C. D. Cappa, J. P. D. Abbatt, Aging of Atmospheric
440 Brown Carbon Aerosol. *ACS Earth Space Chem.* **5**, 722–748 (2021).

441 15. H. Forrister, *et al.*, Evolution of brown carbon in wildfire plumes. *Geophysical Research
442 Letters* **42**, 4623–4630 (2015).

443 16. S. Dasari, *et al.*, Photochemical degradation affects the light absorption of water-soluble
444 brown carbon in the South Asian outflow. *Science Advances* **5**, eaau8066 (2019).

445 17. Y. Chen, *et al.*, Brown carbon in atmospheric fine particles in Yangzhou, China: Light
446 absorption properties and source apportionment. *Atmospheric Research* **244**, 105028
447 (2020).

448 18. S. S. de Sá, *et al.*, Contributions of biomass-burning, urban, and biogenic emissions to the
449 concentrations and light-absorbing properties of particulate matter in central Amazonia
450 during the dry season. *Atmospheric Chemistry and Physics* **19**, 7973–8001 (2019).

451 19. X. Wang, *et al.*, Deriving brown carbon from multiwavelength absorption measurements:
452 method and application to AERONET and Aethalometer observations. *Atmospheric
453 Chemistry and Physics* **16**, 12733–12752 (2016).

454 20. A. L. Hodshire, *et al.*, Aging Effects on Biomass Burning Aerosol Mass and Composition: A
455 Critical Review of Field and Laboratory Studies. *Environ. Sci. Technol.* **53**, 10007–10022
456 (2019).

457 21. R. A. Di Lorenzo, C. J. Young, Size separation method for absorption characterization in
458 brown carbon: Application to an aged biomass burning sample. *Geophysical Research
459 Letters* **43**, 458–465 (2016).

460 22. R. A. Di Lorenzo, *et al.*, Molecular-Size-Separated Brown Carbon Absorption for Biomass-
461 Burning Aerosol at Multiple Field Sites. *Environ. Sci. Technol.* **51**, 3128–3137 (2017).

462 23. R. Zhao, *et al.*, Photochemical processing of aqueous atmospheric brown carbon.
463 *Atmospheric Chemistry and Physics* **15**, 6087–6100 (2015).

464 24. R. F. Hems, J. P. D. Abbatt, Aqueous Phase Photo-oxidation of Brown Carbon Nitrophenols:
465 Reaction Kinetics, Mechanism, and Evolution of Light Absorption. *ACS Earth Space Chem.*
466 **2**, 225–234 (2018).

467 25. Y. Zhang, *et al.*, Top-of-atmosphere radiative forcing affected by brown carbon in the
468 upper troposphere. *Nature Geoscience* **10**, 486–489 (2017).

469 26. N. P. Lareau, C. B. Clements, Environmental controls on pyrocumulus and
470 pyrocumulonimbus initiation and development. *Atmospheric Chemistry and Physics* **16**,
471 4005–4022 (2016).

472 27. C. K. Gatebe, T. Varnai, R. Poudyal, C. Ichoku, M. D. King, Taking the pulse of pyrocumulus
473 clouds. *Atmospheric Environment* **52**, 121–130 (2012).

474 28. F. Dahlkötter, *et al.*, The Pagami Creek smoke plume after long-range transport to the
475 upper troposphere over Europe – aerosol properties and black carbon mixing state.
476 *Atmospheric Chemistry and Physics* **14**, 6111–6137 (2014).

477 29. J. Ditas, *et al.*, Strong impact of wildfires on the abundance and aging of black carbon in
478 the lowermost stratosphere. *PNAS* **115**, E11595–E11603 (2018).

479 30. A. Ansmann, *et al.*, Extreme levels of Canadian wildfire smoke in the stratosphere over
480 central Europe on 21–22 August 2017. *Atmospheric Chemistry and Physics* **18**, 11831–
481 11845 (2018).

482 31. S. S. Petters, S. M. Kreidenweis, A. P. Grieshop, P. J. Ziemann, M. D. Petters, Temperature-
483 and Humidity-Dependent Phase States of Secondary Organic Aerosols. *Geophysical
484 Research Letters* **46**, 1005–1013 (2019).

485 32. L. Renbaum-Wolff, *et al.*, Viscosity of α -pinene secondary organic material and
486 implications for particle growth and reactivity. *PNAS* **110**, 8014–8019 (2013).

487 33. J. Li, S. M. Forrester, D. A. Knopf, Heterogeneous oxidation of amorphous organic aerosol
488 surrogates by O₃, NO₃, and OH at typical tropospheric temperatures. *Atmos. Chem. Phys.*
489 **20**, 6055–6080 (2020).

490 34. T. Koop, J. Bookhold, M. Shiraiwa, U. Pöschl, Glass transition and phase state of organic
491 compounds: dependency on molecular properties and implications for secondary organic
492 aerosols in the atmosphere. *Phys. Chem. Chem. Phys.* **13**, 19238–19255 (2011).

493 35. M. Shiraiwa, *et al.*, Global distribution of particle phase state in atmospheric secondary
494 organic aerosols. *Nat Commun* **8**, 1–7 (2017).

495 36. A. M. Maclean, *et al.*, Global Distribution of the Phase State and Mixing Times within
496 Secondary Organic Aerosol Particles in the Troposphere Based on Room-Temperature
497 Viscosity Measurements. *ACS Earth Space Chem.* **5**, 3458–3473 (2021).

498 37. T. Berkemeier, *et al.*, Ozone uptake on glassy, semi-solid and liquid organic matter and the
499 role of reactive oxygen intermediates in atmospheric aerosol chemistry. *Phys. Chem.
500 Chem. Phys.* **18**, 12662–12674 (2016).

501 38. S. Zhou, M. Shiraiwa, R. D. McWhinney, U. Pöschl, J. P. D. Abbatt, Kinetic limitations in gas-
502 particle reactions arising from slow diffusion in secondary organic aerosol. *Faraday
503 Discuss.* **165**, 391–406 (2013).

504 39. X. Wang, *et al.*, Exploring the observational constraints on the simulation of brown carbon.
505 *Atmospheric Chemistry and Physics* **18**, 635–653 (2018).

506 40. T. S. Carter, *et al.*, Investigating Carbonaceous Aerosol and Its Absorption Properties From
507 Fires in the Western United States (WE-CAN) and Southern Africa (ORACLES and CLARIFY).
508 *Journal of Geophysical Research: Atmospheres* **126**, e2021JD034984 (2021).

509 41. M. Song, *et al.*, Relative humidity-dependent viscosities of isoprene-derived secondary
510 organic material and atmospheric implications for isoprene-dominant forests. *Atmospheric
511 Chemistry and Physics* **15**, 5145–5159 (2015).

512 42. J. J. Schauer, M. J. Kleeman, G. R. Cass, B. R. T. Simoneit, Measurement of Emissions from
513 Air Pollution Sources. 3. C₁–C₂₉ Organic Compounds from Fireplace Combustion of Wood.
514 *Environ. Sci. Technol.* **35**, 1716–1728 (2001).

515 43. L. T. Fleming, *et al.*, Molecular composition and photochemical lifetimes of brown carbon
516 chromophores in biomass burning organic aerosol. *Atmospheric Chemistry and Physics* **20**,
517 1105–1129 (2020).

518 44. S. Net, S. Gligorovski, S. Pietri, H. Wortham, Photoenhanced degradation of veratraldehyde
519 upon the heterogeneous ozone reactions. *Phys. Chem. Chem. Phys.* **12**, 7603–7611 (2010).

520 45. S. Net, E. G. Alvarez, S. Gligorovski, H. Wortham, Heterogeneous reactions of ozone with
521 methoxyphenols, in presence and absence of light. *Atmospheric Environment* **45**, 3007–
522 3014 (2011).

523 46. R. F. Hems, *et al.*, Aqueous Photoreactions of Wood Smoke Brown Carbon. *ACS Earth
524 Space Chem.* **4**, 1149–1160 (2020).

525 47. X. Fan, *et al.*, The evolutionary behavior of chromophoric brown carbon during ozone
526 aging of fine particles from biomass burning. *Atmospheric Chemistry and Physics* **20**, 4593–
527 4605 (2020).

528 48. M. Shiraiwa, M. Ammann, T. Koop, U. Pöschl, Gas uptake and chemical aging of semisolid
529 organic aerosol particles. *PNAS* **108**, 11003–11008 (2011).

530 49. A. M. Maclean, *et al.*, Humidity-Dependent Viscosity of Secondary Organic Aerosol from
531 Ozonolysis of β-Caryophyllene: Measurements, Predictions, and Implications. *ACS Earth
532 Space Chem.* **5**, 305–318 (2021).

533 50. D. R. Worsnop, J. W. Morris, Q. Shi, P. Davidovits, C. E. Kolb, A chemical kinetic model for
534 reactive transformations of aerosol particles. *Geophysical Research Letters* **29**, 57-1-57-4
535 (2002).

536 51. J. W. Morris, *et al.*, Kinetics of submicron oleic acid aerosols with ozone: A novel aerosol
537 mass spectrometric technique. *Geophysical Research Letters* **29**, 71-1-71-4 (2002).

538 52. E. Evoy, S. Kamal, G. N. Patey, S. T. Martin, A. K. Bertram, Unified Description of Diffusion
539 Coefficients from Small to Large Molecules in Organic–Water Mixtures. *J. Phys. Chem. A*
540 **124**, 2301–2308 (2020).

541 53. D. Tarasick, *et al.*, Tropospheric Ozone Assessment Report: Tropospheric ozone from 1877
542 to 2016, observed levels, trends and uncertainties. *Elementa: Science of the Anthropocene*
543 **7**, 39 (2019).

544 54. A. S. Lefohn, *et al.*, Tropospheric ozone assessment report: Global ozone metrics for
545 climate change, human health, and crop/ecosystem research. *Elementa: Science of the*
546 *Anthropocene* **6**, 27 (2018).

547 55. J. Staehelin, W. Schmid, Trend analysis of tropospheric ozone concentrations utilizing the
548 20-year data set of ozone balloon soundings over Payerne (Switzerland). *Atmospheric*
549 *Environment. Part A. General Topics* **25**, 1739–1749 (1991).

550 56. S. Park, S.-W. Son, M.-I. Jung, J. Park, S. S. Park, Evaluation of tropospheric ozone
551 reanalyses with independent ozonesonde observations in East Asia. *Geoscience Letters* **7**,
552 12 (2020).

553 57. S. Sandroni, D. Anfossi, Trend of Ozone in the free troposphere above Europe. *Il Nuovo*
554 *Cimento C* **18**, 497–503 (1995).

555 58. S. Shi, *et al.*, Biomass burning aerosol characteristics for different vegetation types in
556 different aging periods. *Environment International* **126**, 504–511 (2019).

557 59. X. Yu, *et al.*, Aerosol optical properties during firework, biomass burning and dust episodes
558 in Beijing. *Atmospheric Environment* **81**, 475–484 (2013).

559 60. K. O. Ogunjobi, Z. He, K. W. Kim, Y. J. Kim, Aerosol optical depth during episodes of Asian
560 dust storms and biomass burning at Kwangju, South Korea. *Atmospheric Environment* **38**,
561 1313–1323 (2004).

562 61. C. Papastefanou, Residence time of tropospheric aerosols in association with radioactive
563 nuclides. *Applied Radiation and Isotopes* **64**, 93–100 (2006).

564 62. T. Tokieda, K. Yamanaka, K. Harada, S. Tsunogai, Seasonal variations of residence time and
565 upper atmospheric contribution of aerosols studied with Pb-210, Bi-210, Po-210 and Be-7.
566 *Tellus B* **48**, 690–702 (1996).

567 63. M. J. Iacono, *et al.*, Radiative forcing by long-lived greenhouse gases: Calculations with the
568 AER radiative transfer models. *Journal of Geophysical Research: Atmospheres* **113** (2008).

569 64. C. L. Heald, *et al.*, Contrasting the direct radiative effect and direct radiative forcing of
570 aerosols. *Atmospheric Chemistry and Physics* **14**, 5513–5527 (2014).

571 65. J. Li, D. A. Knopf, Representation of Multiphase OH Oxidation of Amorphous Organic
572 Aerosol for Tropospheric Conditions. *Environ. Sci. Technol.* **55**, 7266–7275 (2021).

573 66. M. L. Hinks, *et al.*, Effect of viscosity on photodegradation rates in complex secondary
574 organic aerosol materials. *Phys. Chem. Chem. Phys.* **18**, 8785–8793 (2016).

575 67. B. J. Murray, *et al.*, Heterogeneous nucleation of ice particles on glassy aerosols under
576 cirrus conditions. *Nature Geosci* **3**, 233–237 (2010).

577 68. M. J. Wolf, *et al.*, A biogenic secondary organic aerosol source of cirrus ice nucleating
578 particles. *Nat Commun* **11**, 4834 (2020).

579 69. A. Trofimova, R. F. Hems, T. Liu, J. P. D. Abbatt, E. G. Schnitzler, Contribution of Charge-
580 Transfer Complexes to Absorptivity of Primary Brown Carbon Aerosol. *ACS Earth Space
581 Chem.* **3**, 1393–1401 (2019).

582 70. E. Evoy, *et al.*, Diffusion Coefficients and Mixing Times of Organic Molecules in β -
583 Caryophyllene Secondary Organic Aerosol (SOA) and Biomass Burning Organic Aerosol
584 (BBOA). *ACS Earth Space Chem.* **5**, 3268–3278 (2021).

585 71. R. W. Hyland, A. Wexler, Formulation for the thermodynamic properties of the saturated
586 phases of H₂O from 173.15 K to 473.15 K. *ASHRAE Trans.* **89**, 500–519 (1983).

587 72. J. W. Grayson, M. Song, M. Sellier, A. K. Bertram, Validation of the poke-flow technique
588 combined with simulations of fluid flow for determining viscosities in samples with small
589 volumes and high viscosities. *Atmospheric Measurement Techniques* **8**, 2463–2472 (2015).

590 73. X. Wang, *et al.*, Exploiting simultaneous observational constraints on mass and absorption
591 to estimate the global direct radiative forcing of black carbon and brown carbon.
592 *Atmospheric Chemistry and Physics* **14**, 10989–11010 (2014).

593 74. R. Saleh, *et al.*, Brownness of organics in aerosols from biomass burning linked to their
594 black carbon content. *Nature Geosci* **7**, 647–650 (2014).

595

596

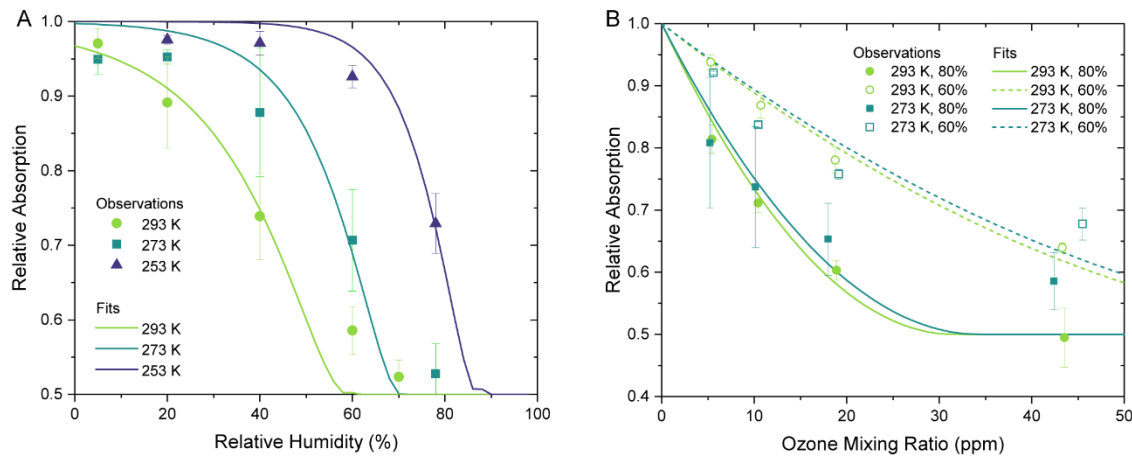
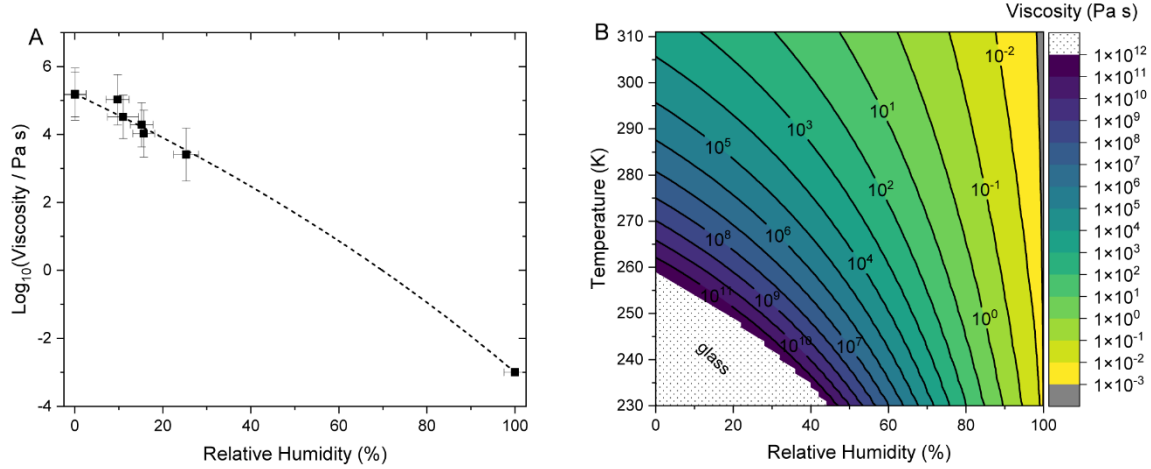
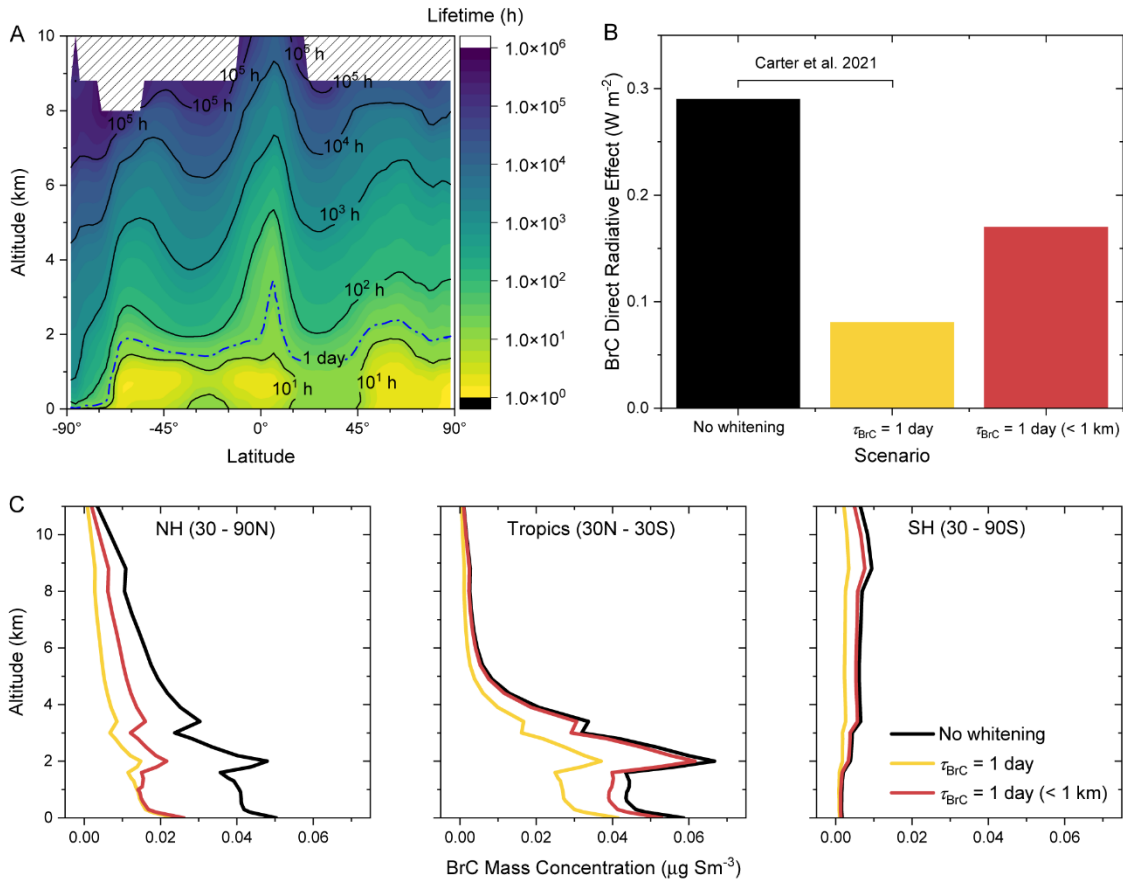
Figures

Fig. 1. Relative absorption at 405 nm remaining (A) after exposure to 45 ppm of ozone as a function of RH at 253, 273, and 293 K and (B) as a function of ozone mixing ratio at either 273 or 293 K and 60 or 80% RH. The curves represent fits of Eq. 2 to the experimental data points. Error bars represent one standard deviation of four sets of datapoints.



606
 607 **Fig. 2.** Panel (A) shows viscosities of the BBOA as a function of RH. Symbols show the averages
 608 of the $\log(\text{viscosity})$ values, with y -error bars representing the upper and lower limits at each RH
 609 and x -error bars representing the uncertainty in RH. Data for both 10 mL and 50 mL water extracts
 610 are shown (Fig. S6). Included at RH of 100% is the viscosity of pure water at a temperature of 294
 611 K. The black dashed curve corresponds to a fit to the data using the parameterization (SI Appendix,
 612 section S1). Panel (B) shows predicted viscosities of BBOA as a function of temperature and RH.
 613 Viscosities above 10^{12} Pa s correspond to a glass state and are cut off (hatched region) because
 614 they are not modelled well by the Vogel-Fulcher-Tamman equation.
 615
 616

617
618



619
620
621
622
623
624
625
626
627
628
629
630
631

Fig. 3. Panel (A) shows the predicted annual average lifetimes of water-soluble BrC in the atmosphere as a function of altitude and latitude. The dashed blue line represents 1-day whitening of BrC. Panel (B) shows the global mean all-sky top-of-atmosphere BrC direct radiative effect (DRE) in 2018 for the schemes with no-whitening, 1-day whitening, and 1-day whitening only below 1 km. The third scheme is new to this study; the first two schemes are described in Carter et al. (40). Panel (C) shows the simulated mean 2018 BrC mass concentrations by altitude for the three schemes in panel (B). BrC mass concentrations are reported at standard conditions of temperature and pressure (STP: 273K, 1 atm).